Materials Today Sustainability 19 (2022) 100158

Contents lists available at ScienceDirect

Materials Today Sustainability

journal homepage: https://www.journals.elsevier.com/materials-today-sustainability

A rotational switched-mode water-based triboelectric nanogenerator for mechanical energy harvesting and vehicle monitoring

C.-D. Le [a], T.-H. Nguyen [a], D.-L. Vu [a], C.-P. Vo [b], K.K. Ahn [c, *]

[a] Graduate School of Mechanical Engineering, University of Ulsan, Republic of Korea
[b] School of Electrical Engineering, Ulsan National Institute of Science and Technology (UNIST), Republic of Korea
[c] School of Mechanical Engineering, University of Ulsan, Republic of Korea

ARTICLE INFO

Article history:
Received 1 March 2022
Received in revised form
15 April 2022
Accepted 29 April 2022
Available online 14 May 2022

Keywords:
Triboelectric nanogenerator
Water electrification
Mechanical switch
Self-sensing device
Vehicle monitoring

ABSTRACT

Nowadays, vehicles are involved deeply in human life, especially for passengers and goods transportation, and along with technological advancements, the autonomous car becomes one of the most concerning issues. With the aim of management and control, many kinds of sensors are situated in different parts of the vehicle to ensure safe and reliable driving, but they also drain out more power from the electric circuit. In this work, a rotational switched-mode water-based triboelectric nanogenerator (RSW-TENG) as battery-free device is demonstrated, in which its capability of converting rotational kinetic energy into electricity and detecting the road slope as well as the wheel speed is carefully investigated. The spatial relation between water and electrodes during operation has a great effect on the electrical outputs of RSW-TENG where they represent a negative proportional relationship with the slope angle ranging from 0° to 80°; meanwhile, a positive proportional relationship with rotational speed is observed instead. The practical evaluation with a prototype of vehicle wheel attached RSW-TENG is implemented, and it exhibits a reliable and accurate performance under different inclinations and driving speeds. These results point out that the RSW-TENG could be an appropriate selection for monitoring and enhancing driving safety.

1. Introduction

For a long time, vehicles have played an important role in our modern society because they are a must-use for delivering passengers and goods to precise destinations; hence, driving has become a vital part of human life. Along with the digital revolution, cars equipped with driver assistance systems, and later, automated driving systems have been introduced and continuously improved by which to shorten the gap toward fully autonomous cars. For acquiring this target, more and different kinds of sensors are being situated in different parts of the vehicle to monitor its operating, thereby guaranteeing safety and reliable driving [1,2]. However, the installation of auxiliary sensing devices, which means extra power consumption, certainly adds more stress to the energy supply system that is currently based on battery circuits. By the day, thanks to the technological advances, the size and power consumption of up-to-date sensors are significantly decreased, but the maintenance costs, environmental hazards, and complexity of battery-operated devices remain relatively high, leading to the persistent challenge for the development of various sustainable energy technologies [3,4]. Among them, self-powered sensing technology is heading for as a succeeding solution, where environmental energy harvesting is required [5–7]. Waste mechanical energies are a good choice due to their ubiquity and availability and have attracted many researchers around the world so far [8–12]. Different types of energy conversion mechanisms, such as electromagnetic, piezoelectric, thermoelectric, and pyroelectric, have been investigated and applied to scavenge these waste energies with excellent achievements [13–17].

In the past decade, triboelectric nanogenerators (TENGs) were invented and set a whole new way of harvesting ambient mechanical energy. By coupling the triboelectric effect and electrostatic induction, the electricity can be generated through the physical contact and separation between two surfaces having different triboelectric properties. They have the edge over other generators, featuring lightweight, vast materials selection, ease of fabrication, and high efficiency even at low operation frequency, which have gained a lot of attention in recent years [18–21]. With regard to the light-duty transportation safety aspect, there are

* Corresponding author.
E-mail address: kkahn@ulsan.ac.kr (K.K. Ahn).

https://doi.org/10.1016/j.mtsust.2022.100158
2589-2347/

many interesting works where TENGs were introduced as self-powered sensors for monitoring real-time operating conditions of vehicle [22–29]. Most of the reported TENGs for vehicle sensing application rely entirely on the solid-solid contact electrification principle and show great results; nevertheless, the solid-based TENGs still remain some limitations [30]. Meanwhile, it is realized that the triboelectrification even occurs at the water-solid interface [31]; hence, water-based TENGs progressively get more notice and are available for competing in the self-powered sensing application [32–35].

In this study, a rotational switched-mode water-based triboelectric nanogenerator (RSW-TENG) is presented and examined for harvesting the rotational kinetic energy of the wheel. The RSW-TENG is composed of a water-filled cylindrical TENG with PTFE as solid-phase triboelectric material, in which every single electrode is split into two portions, one portion as the rotating electrode (RE) and the other as the stationary electrode (SE). When the cylindrical component rotates as well as the RE, the RSW-TENG is typically isolated with an external circuit except at designated locations where the RE adjoins the SE every half cycle. This allows the RSW-TENG to accumulate induced charges and instantly releases them following the closed-circuit state so that the output current could enhance significantly. Additionally, owning to the conditional conductive of RSW-TENG, the relative position of the electrode with respect to water in the closed-circuit interval has a relevant impact on the output performance. Thereby, the angular sensing has been verified with good stability and sensitivity, which represents the capability of RSW-TENG as a road slope sensor.

2. Results and discussion

Fig. 1a exhibits the structure of RSW-TENG, including a rotating cylinder and a support stand. Two semicircle copper foils as electrode layer and a circle PTFE membrane as dielectric layer are sequentially secured inside the cylinder to complete the solid phase of TENG. The deionized (DI) water is selected for the liquid phase of the TENG and poured into the cylinder until it totally covers an electrode surface. Subsequently, two small pieces of copper are symmetrically adhered to the cylinder, and each one connects to a corresponding semicircle electrode to finalize a pair of RE. Another two small pieces of copper are symmetrically fixed on the support holder as a couple of SE so that each RE consciously pairs up with a RE at the same time every half-cycle as shown in Fig. 1b. This setup, called a discontinuous conduction circuit, only allows the current passing through the external load at specific geometrical locations, by which the charge transfer between electrodes would be pending until a full electric connection is established. During rotation, the water remains static due to gravitational force; meanwhile, the PTFE membrane and the REs move along with the cylinder in synchronous speed. Then, the overlapping area between water and each RE at the closed-circuit condition certainly affects the electrical output performance which will be discussed later.

The working principle of RSW-TENG derives from the sliding freestanding mode, in which PTFE is selected as the triboelectric counterpart in the water contact electrification. The PTFE is chosen as the friction layer due to its high negativity in the triboelectric series which prefers to gain triboelectric charges, along with high volume and surface resistance as well as excellent water repellency which helps the tribo-charges remain on the surface for a long time, extending the working life of friction layer. A full running cycle of RSW-TENG is depicted in Fig. 2 and described as follows. Initially, since water is in contact with the PTFE membrane, the opposite polarity occurs at the water-PTFE interface such that the PTFE surface becomes negatively charged and the water surface becomes positively charged. This appearance can be explained by means of charge distribution at solid-liquid interfaces following the “two-step” model [36] or Wang's hybrid layer [37]. As the cylinder rotates, the overlapping area between water and each electrode has a change with an increment for one electrode and a decrement for the other electrode so that the electric potential difference between the two electrodes is gradually developed (Fig. 2-ii). It happens until the closed-circuit condition is established, inducing a charge transfer from the former electrode to the latter one (Fig. 2-iii). The presence of induced current also concludes the first half cycle of RSW-TENG operation, and the new electrostatic equilibrium arises. It is recognized that the closed-circuit state just occurs in a very short time; therefore, charge leakage and impedance mismatch could be minimized to enhance the electrical output of the TENG. In the second half cycle, once the TENG backs to off-state, the charge flow is terminated appropriately such that no current signal could be observed, and the functionality of each electrode relative to water is interchanged following the TENG rotation concurrently (Fig. 2-iv). During this stage, the electric potential difference turns up again after the charge balance breakdown and arouses a current flowing through the external circuit as soon as the electrical conduction is exposed (Fig. 2-i). These steps already reveal a complete operating cycle of RSW-TENG, and the next cycles could be perceived likewise. Furthermore, the course of transferred charges across the external load is always unchanged according to the symmetrical alignment of SE in the company with static water, which literally ends up with a unidirectional current. It is realized that the on-state potential difference, i.e., output voltage, depends on the relative position of dual electrodes with respect to water, which is defined as a phase angle. To more extent, the output voltage of RSW-TENG could be expressed by the following relation.

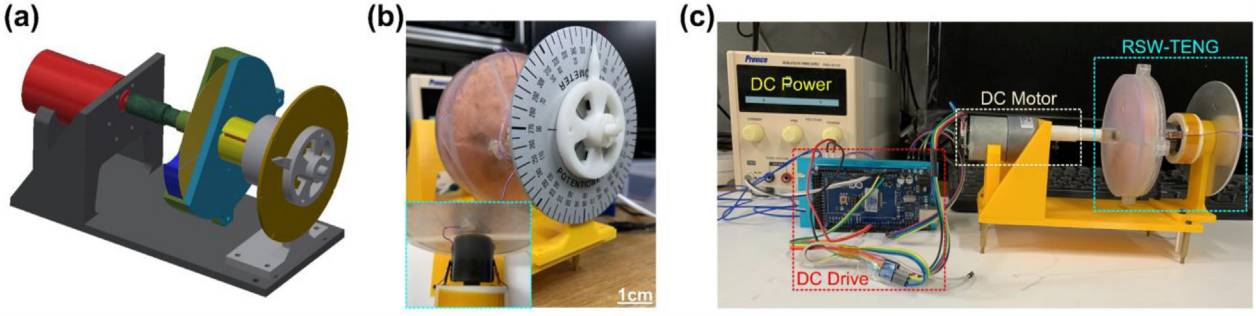

Fig. 1. (a) Conceptual design and (b) practical implementation of the RSW-TENG (scale bar: 1 cm). Inset: electrode pairings for rotational switched-mode conduction. (c) Experimental setup for electrical characterization.

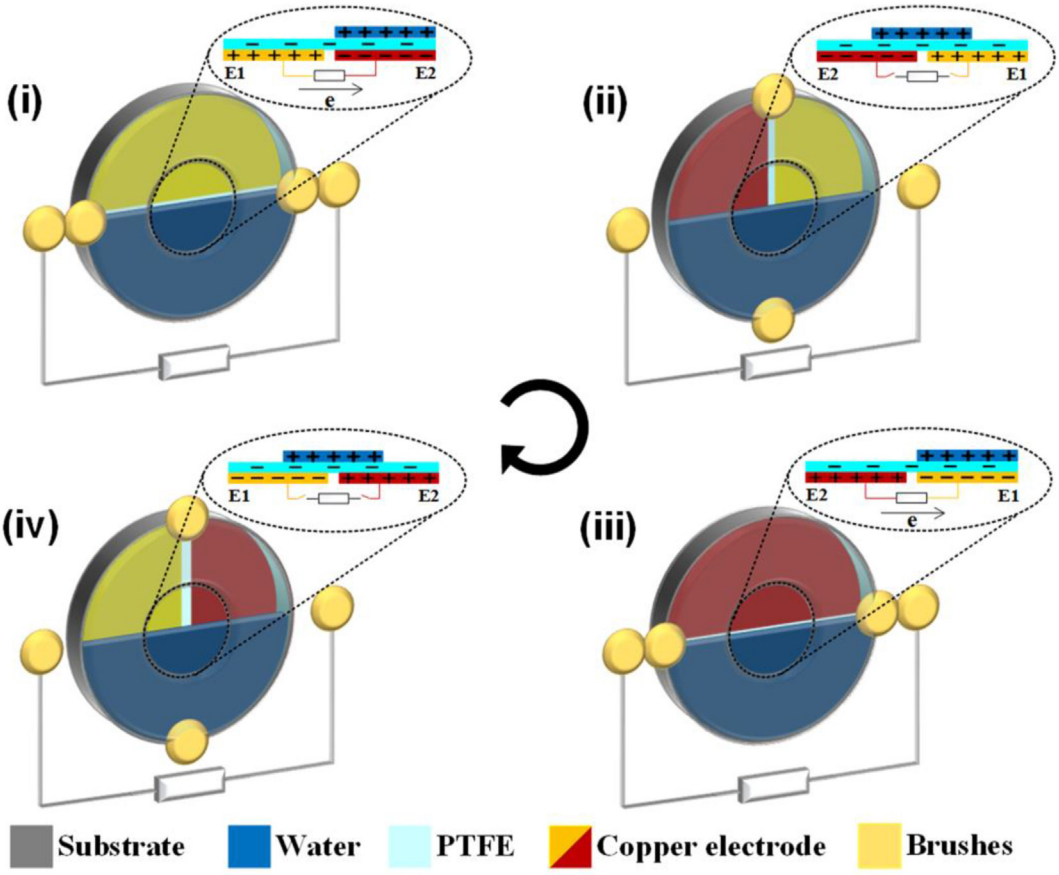

Fig. 2. Relative position of each electrode with respect to the water and working principle of the RSW-TENG in one cycle of revolution.

$$V_0 = \frac{\sigma \pi r^2}{2C} \tag{1}$$

where σ is the tribo-charge density, r is the radius of semicircle electrode, and C is the on-state capacitance of the RSW-TENG. In this configuration, the on-state capacitance C is the serial connection of C_1 and C_2, where C_1 and C_2 are equivalent capacitance between each electrode and water. So, at an arbitrary phase angle θ, C_1 and C_2 are given by

$$\begin{cases} C_1 = \dfrac{\varepsilon_0 \varepsilon_r \theta r^2}{2d} \\ C_2 = \dfrac{\varepsilon_0 \varepsilon_r (\pi - \theta) r^2}{2d} \end{cases} \tag{2}$$

where ε_0 is the permittivity of free space, ε_r is the relative permittivity of dielectric membrane, and d is the thickness of dielectric membrane. Finally, C is obtained as

$$C = \frac{\varepsilon_0 \varepsilon_r r^2}{2\pi d}\left(\pi\theta - \theta^2\right) \tag{3}$$

Thus, it is evident that the output voltage of RSW-TENG decreases corresponding to the increment of phase angle as well as on-state capacitance. Accordingly, a slope angle sensing device can be adopted by taking advantage of this property.

For further investigation into the empirical performance of RSW-TENG, a variable-speed DC motor is utilized to drive the rotary cylinder either clockwise or counterclockwise (Fig. 1c). In relation to basic demonstration, the phase angle is set to be zero degree together with the rotation speed of 1.25 Hz, by which the water body could fully cover an electrode at closed-circuit condition. Fig. 3a–b shows the output voltage and output current corresponding to the relevant settings with peak voltage of 1.78 V and peak current of 0.91 μA, respectively. It is visible that both electric signals are unidirectional and come up with a spike waveform such that the value sharply increases from zero to maximum and then decreases back to zero in a short time. Additionally, there are two spikes to be recorded in one revolution of the RSW-TENG, which successfully verifies the operating mechanism. Alongside, the electrical output in the case of clockwise rotation is alike those in the case of counterclockwise rotation, thanks to the rational coupling of SE and RE. As depicted in Fig. 2, at the conducting point, the RE covered by water always connects to the left SE; meanwhile, the exposed RE consistently joins to the right SE so that the electric charges just traverse the external circuit on one-way path regardless of rotational direction. From Eq. (1), the maximum output voltage indicates a linearly proportional relation to the accumulated charge density, which varies very little during operation but does not affect by external resistance. Thereby, the peak output voltage shows a nearly unchanged peak magnitude (approximately ranging from 1.68 V to 1.82 V), despite the change of resistor as illustrated in Fig. 3c. In relevance, the peak output current with respect to resistance turns out an inversely proportional relationship, in which its power level drops down from 0.91 μA at 20 MΩ to 0.18 μA at 100 MΩ. Likewise, the peak output power is subjected to load change such that it reduces from 1.59 μW to 0.31 μW when the resistance increases from 20 MΩ to 100 MΩ. Hence, it implies that the RSW-TENG can deliver power more effectively when operating at low load resistance. The output power of the RSW-TENG can use to charge capacitors without the necessity of a rectifier circuit (Fig. 3d)

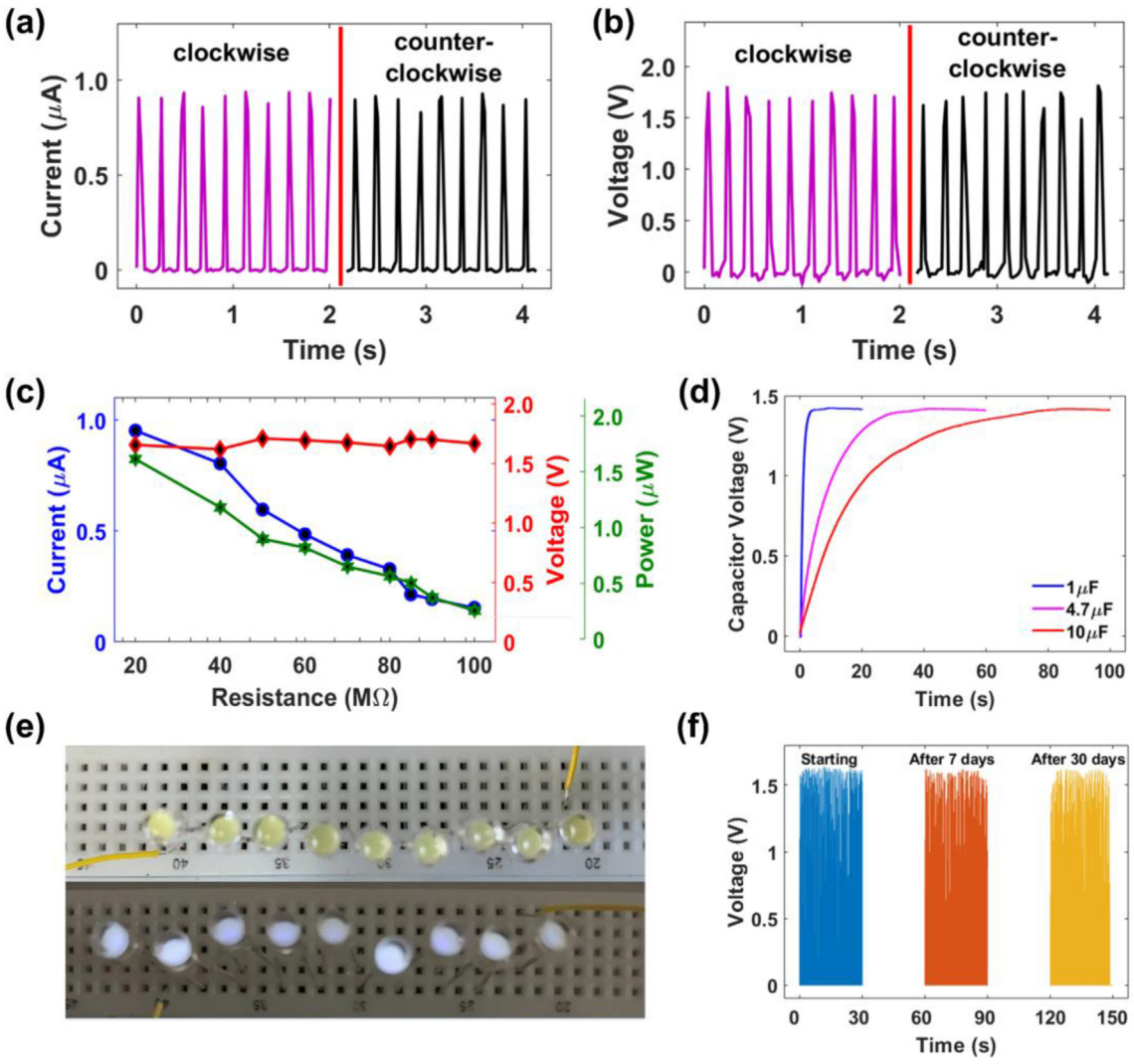

Fig. 3. Electrical characterization of the RSW-TENG as to phase angle of zero degree and rotating speed of 1.25 Hz. (a) Output current and (b) output voltage regarding clockwise and counterclockwise rotation. (c) Peak output current, peak output voltage, and peak output power under different load resistances. (d) Demonstration of charging different capacitors. (e) Demonstration of continuously lighting up LEDs in series. (f) Durability and stability of the RSW-TENG over time.

or directly light up several LEDs in series (Fig. 3e and Supporting Video S1). Here, the maximum charging voltage is up to 1.41 V for every tested capacitor with the settling time of 5.63 s, 38.22 s, and 85.76 s with regard to the capacitance of 1 μF, 4.7 μF, and 10 μF, respectively. Besides, as shown in Fig. 3f, the RSW-TENG ensures good durability and stability over time in which the output voltage just suffers a degradation by less than 1% after 30 days of operation. Through these inspections, it turns out that the RSW-TENG possesses the necessary attributes to be developed into a self-powered device.

Supplementary video related to this article can be found at https://doi.org/10.1016/j.mtsust.2022.100158

As mentioned previously, the phase angle of RSW-TENG, as defined in Fig. 4a and Fig. S1 (Supporting Information), has a significant impact on the output voltage and output current such that it directly quantifies the intrinsic capacitance as derived in Eq. (3). On closer inspection, the output current and voltage are measured under various phase angles under common rotating speed of 1.25 Hz, in which the SE is predefined at a specific slope compared to the static water level. As demonstrated in Fig. 4b–c, the electrical output has a descending tendency regarding the ascending order of slope such that the output current degrades steadily from 0.91 μA at null degree to 0.08 μA at 80°. Simultaneously, the output voltage loses its power by roughly 88%, downgrading from 1.78 V to 0.21 V when the slope changes from zero degree to 80°, respectively. Here, the quantitative relationship between voltage peak and slope angle can be obtained through a linear regression analysis and yielding

$$V_0 = \frac{0.6319}{\pi\theta - \theta^2}$$

This expression thus complies with the Eq. (1). Apparently, phase angle would determine the effective covered area of both electrodes and thus the on-state dielectric capacitance of RSW-TENG. Suppose that a constant tribo-charge density is held, and the rise of on-state capacitance leads to the deficiency of electric field across two electrodes, resulting in a falloff in potential difference. Therefore, the incremental change to phase angle, which increases the on-state capacitance correspondingly, could inflict an appropriate turn-down on the output voltage and output current of the RSW-TENG. Besides, the charge accumulation in a 10 μF capacitor under different phase angles is also examined and depicted in Fig. 4d, and it is obvious that the larger phase angle, the less charge accumulated on the capacitor. From another

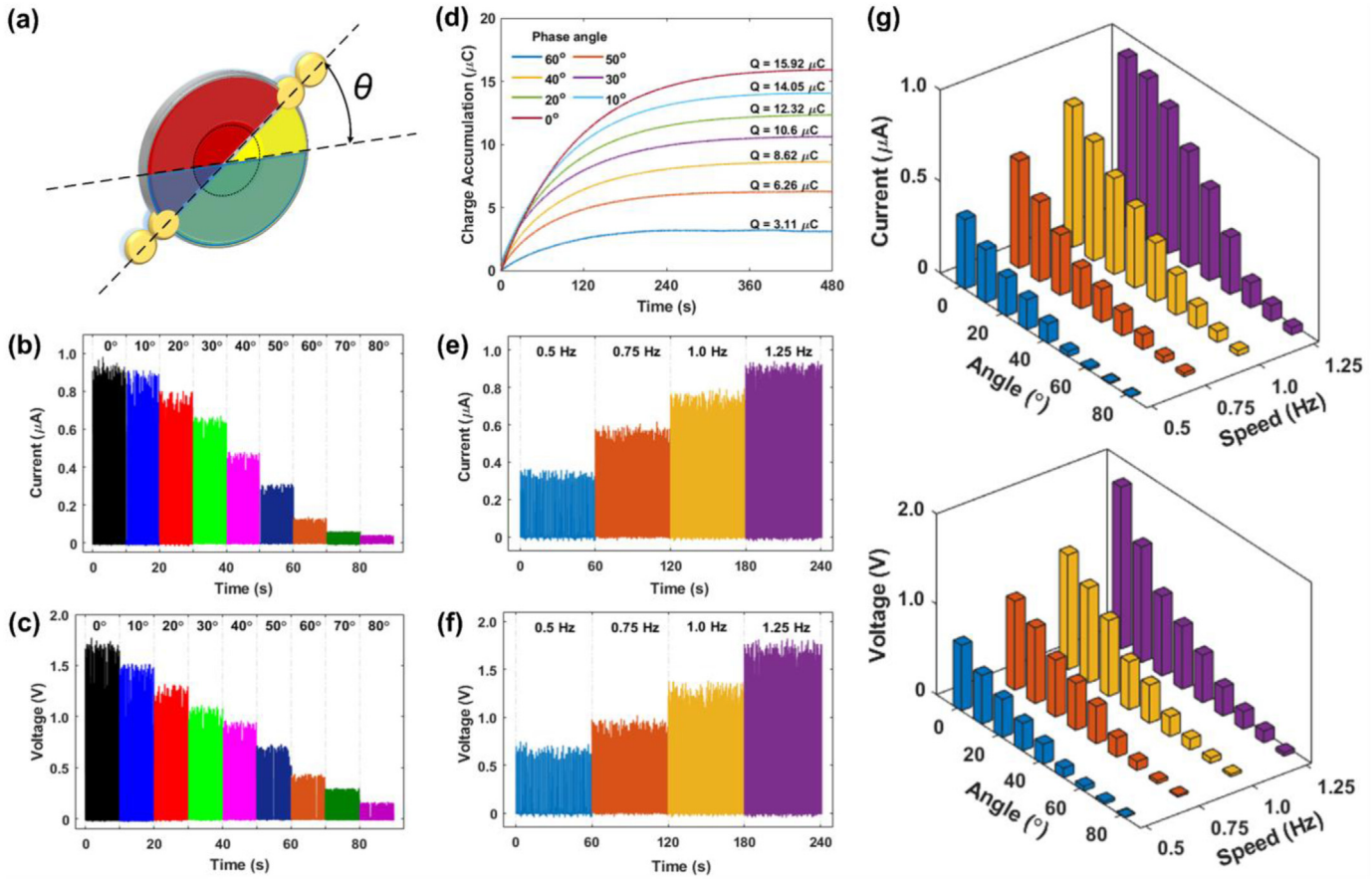

Fig. 4. Electrical output performance of RSW-TENG under different phase angle and rotating frequency. (a) Phase angle definition as the angle difference between water line and stationary electrodes line. (b, c) Current and voltage with phase angle from 0° to 80° at running speed of 1.25 Hz. (d) Charge accumulation on 10 μF capacitors at different phase angle. (e, f) Current and voltage with rotating frequency from 0.5 Hz to 1.25 Hz at phase angle of 0°. (g) 3D graph of output current and output voltage under effect of both phase angle and rotating frequency.

perspective, the electrical output of RSW-TENG shows up a linearly proportional relationship with respect to the increase of rotating frequency, as can be seen in Fig. 4e–f. During observation, the phase angle is locked up such that it remains constant at zero degree. Starting from 0.5 Hz, the rotating frequency ramps up step by step and lastly achieves the highest speed of 1.25 Hz which is in association with the enhancement of peak output current from 0.38 μA to 0.91 μA and peak output voltage from 0.71 V to 1.78 V. This is because more opposed charges on the dielectric surface due to screen effect should be swept away as the rotating speed increases, which amplifies the potential difference along with the transferred charge between electrodes. Thus, it is inferred that the output current and output voltage could be improved by boosting the rotating speed. However, due to the physical limits of the testbench assembly, the RSW-TENG is restricted to the running speed of 1.5Hz for preventing the dispersion of water which probably distorts the output current. Further, a thorough relation of output characteristics of RSW-TENG with phase angle and rotating frequency is presented in Fig. 4g. Obviously, the issue of short on electrical output at a larger phase angle can be overcome by increasing the rotating speed; however, up to a certain limitation, this compensation becomes less appreciable.

The RSW-TENG features a clear sensitivity to the variation of phase angle and rotating speed that fairly qualifies for road slope sensing in the vehicle monitoring system. It is pointed out in many studies that the road slope has a significant impact on the vehicle speed and the engine load, in which gravitational force decelerates the vehicle when moving upward (i.e., the engine works more) and accelerates the vehicle when moving downward (i.e., the brake is applied more). Therefore, it is necessary to determine the slope of the roadway for improving safe driving and fuel economy. For further examination, a prototype of vehicle wheel attached RSW-TENG (wheel diameter of 135 mm) is constructed, as depicted in Fig. S2 (Supporting Information), to specify the sensing attribute regarding diverse input where the sensing signal can be analyzed and displayed later after passing through a data acquisition (DAQ) device. As illustrated in Fig. 5a, through the sliding mechanic, the cylinder component of RSW-TENG keeps synchronously rotating along with the wheel so that it can continuously generate the electric signal. During excitation, two SEs are always aligned parallel to the road surface no matter what the slope is; thus, the RSW-TENG can sense the change of road slope in relation to the change of phase angle when the vehicle goes uphill or downhill (Supporting Video S2). In particular performing analysis, the wheel prototype is manipulated at a constant speed of 0.1 m/s on a linear slide rail with the length of 1.8 m, and this setup is consistently experienced in the following occasions. Firstly, in the case of 10-degree road slope (Fig. 5b), the quantized voltage with eight consecutive peaks is recognized with the mean peaks value of 1.15 V. Subsequently, in Fig. 5c–d, the representational voltage for the 20-degree slope and 30-degree slope is exhibited in which the 20-degree test ends up with the mean peaks value of 1.01 V; meanwhile, the mean peaks value of 0.88 V is obtained subject to 30-degree test. The mean squared error (MSE) and standard deviation (STD) as regards each measurement acquire 0.203% and 0.048 V for 10-degree slope, 0.108% and 0.035 V for 20-degree slope, as well as 0.033% and

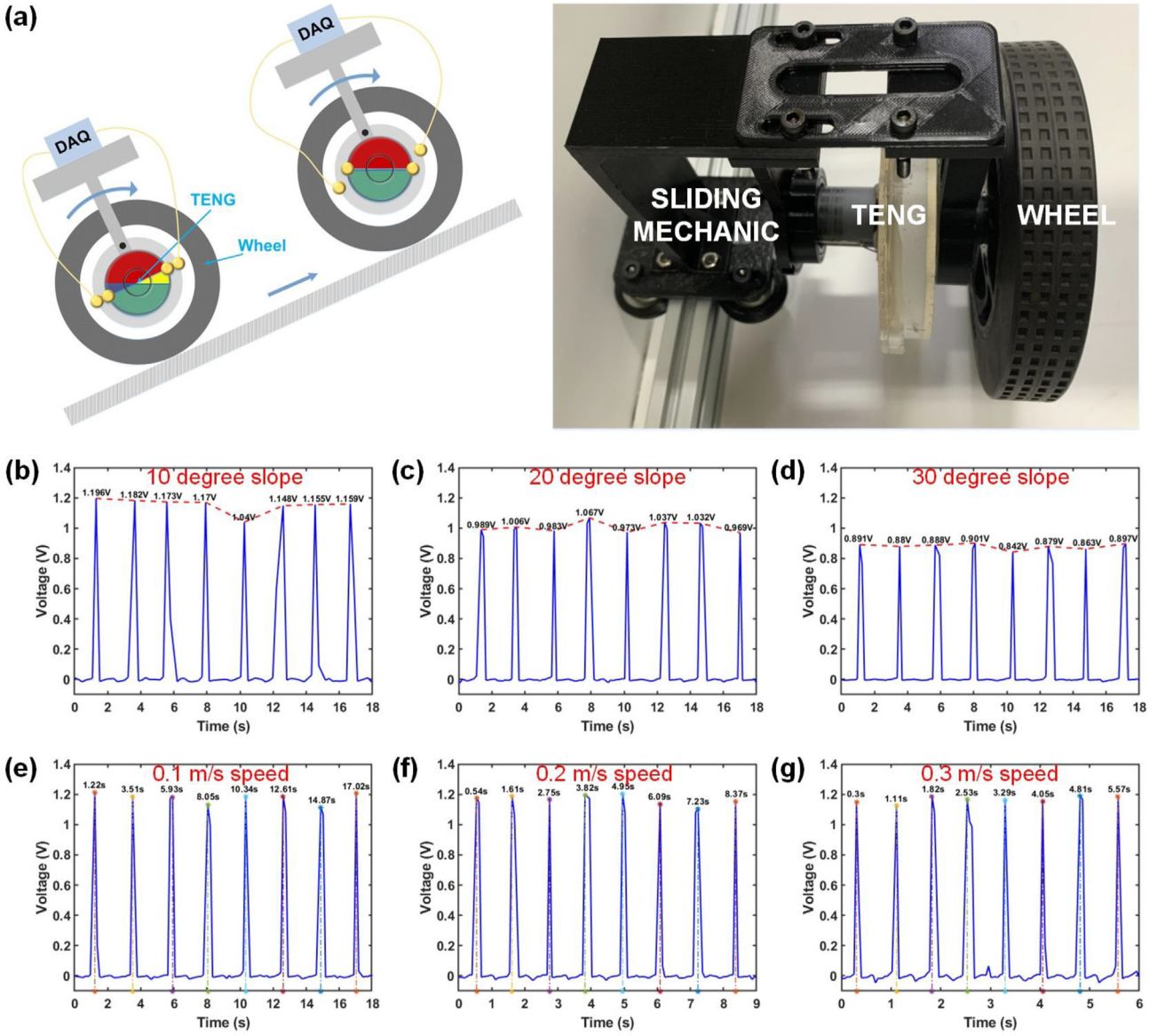

Fig. 5. Application of RSW-TENG as road slope and wheel speed detector. (a) Illustration and prototype of road slope and wheel speed detection for vehicle monitoring using RSW-TENG. The sensing signal is collected and processed through a DAQ device. (b–d) The voltage signal corresponding to different slopes. (e–g) The voltage signal with time difference regarding the different running speed of the prototype.

0.019 V for 30-degree slope. Owning to small MSE and acceptable STD during operation, the RSW-TENG shows good reliability and high accuracy to the road slope detection task. Besides, experiments about wheel speed monitoring are conducted where the rotational speed of the wheel is measured with respect to the acceleration of the prototype. Fig. 5e presents the characterized voltage of the wheel as the prototype is driven at the translational speed of 0.1 m/s, where the wheel rotational speed ω_{wheel} can be approximated by the function $\omega_{wheel} = \pi/\Delta T_{p\text{-}p}$ ($\Delta T_{p\text{-}p}$ is time difference between two consecutive peaks). Based on the approximation, the mean speed value of 1.394 rad/s is observed with the corresponding MSE of 0.319% and STD of 0.061 rad/s. When the prototype is leveled up its speed to 0.2 m/s (see Fig. 5f), the running wheel gets the mean speed value of 2.812 rad/s in relevance to the MSE of 0.621% and STD of 0.085 rad/s. Once the prototype reaches the rate of 0.3 m/s, the wheel concludes with the mean speed value of 4.182 rad/s in addition to the MSE of 2.907% and STD of 0.184 rad/s as displayed in Fig. 5g. Obviously, the wheel speed detection has fairly good reliability and accuracy; and in association with the road slope detection, they can bring about a promising approach in-vehicle safety monitoring systems.

Supplementary video related to this article can be found at https://doi.org/10.1016/j.mtsust.2022.100158

3. Conclusion

In brief, this paper introduces the RSW-TENG as an active transducer for harvesting the rotational kinetic energy of the wheel in addition to the ability of road slope and wheel speed detection. The RSW-TENG is a rotary cylindrical TENG in combination with rotating SE pairings where the electrical output is affected by the spatial alignment of these electrode pairings as well as the rotating speed of TENG. Particularly, the electrical output demonstrates an inversely proportional relationship to the phase angle but in

proportion to the rotating speed, in which the peak current of 0.91 μA and the peak voltage of 1.78 V are recorded under the operational condition of 1.25 Hz and zero-degree gradient. Alongside, the RSW-TENG has the capability of lighting up several LEDs and charging up to 1.41 V for different capacitors at the same condition. Later, based on the established relationship, the RSW-TENG is secured to a wheel model for evaluating the slope and speed detection functionality. For slope detection, the average peak voltage of 1.15 V, 1.01 V, and 0.88 V are realized with respect to 10-degree, 20-degree, and 30-degree angles, respectively. For speed detection, the average rotational speed of the wheel indicates sequentially as 1.394 rad/s, 2.812 rad/s, and 4.182 rad/s for the corresponding speed of 0.1 m/s, 0.2 m/s, and 0.3 m/s. In both cases, the RSW-TENG shows up good reliability and accuracy in its performance, which provides a high potential solution for road slope sensing and wheel speed sensing in-vehicle monitoring systems.

4. Experimental section

4.1. Fabrication of the RSW-TENG

The RSW-TENG is assembled from two subunits, specifically as a rotating unit and a stationary unit. The rotating unit is an enclosed cylinder with a diameter of 90 mm and a depth of 12 mm. Two identical semicircle copper foils with the radius of 43 mm are secured opposite to each other on an inside base of the cylinder, regarding the gap of 2 mm; then, two small pieces of copper are separately coupled with each copper foil through a wired connection to complete the rotary electrode element. A PTFE membrane circle of 90 mm diameter is subsequently bonded over the copper layer, followed by the filling of water inside the cylinder. The water is deposited up to about half-filled capacity of the cylinder such that it would entirely cover a semicircle electrode if they are in parallel. The stationary unit is vertical mounting support with two pieces of copper attached in line with each other as SE elements. Finally, the cylinder and its support are put together with the help of an equipped ball bearing for smooth-running work.

4.2. Characterization of the RSW-TENG

To implement electrical measurement, a DC geared motor (GB37Y3530−12V-90EN, China) with a driver (Motorbank DMD-400, Korea) was used to drive the TENG. The output voltage and output current of the TENG were measured using a digital multimeter (Keithley DMM7510, USA) and a low-noise current preamplifier (Stanford Research Systems SR570, USA) with the load resistance of 20 MΩ. An electrometer (Keithley 6517B, USA) was used to measure net charges on the capacitor. An Arduino Mega was used in associated with the driver to control the DC motor as well as collect the data from the TENG device in actual wheel experiments.

Credit author statement

Chau-Duy Le: conceptualization, writing - original draft, investigation, methodology.

Thanh-Ha Nguyen: methodology, resources.

Duy-Linh Vu: validation, formal analysis, writing - review & editing.

Cong-Phat Vo: investigation, software.

Kyoung Kwan Ahn: supervision, project administration, funding acquisition.

Declaration of competing interest

The authors declare that they have no known competing financial interests or personal relationships that could have appeared to influence the work reported in this paper.

Acknowledgments

This research was supported by Basic Science Research Program through the National Research Foundation of Korea (NRF) funded by the Ministry of Science and ICT, South Korean (NRF-2020R1A 2B5B03001480).

Appendix A. Supplementary data

Supplementary data to this article can be found online at https://doi.org/10.1016/j.mtsust.2022.100158.

References

[1] H. Askari, E. Hashemi, A. Khajepour, M.B. Khamesee, Z.L. Wang, Towards self-powered sensing using nanogenerators for automotive systems, Nano Energy 53 (2018) 1003−1019, https://doi.org/10.1016/j.nanoen.2018.09.032.
[2] H. Askari, A. Khajepour, M.B. Khamesee, Z.L. Wang, Embedded self-powered sensing systems for smart vehicles and intelligent transportation, Nano Energ. 66 (2019) 104103, https://doi.org/10.1016/j.nanoen.2019.104103.
[3] L. Jin, B. Zhang, L. Zhang, W. Yang, Nanogenerator as new energy technology for self-powered intelligent transportation system, Nano Energ. 66 (2019) 104086, https://doi.org/10.1016/j.nanoen.2019.104086.
[4] Z. Wu, T. Cheng, Z.L. Wang, Self-powered sensors and systems based on nanogenerators, Sensors 20 (2020) 2925, https://doi.org/10.3390/s20102925.
[5] A. Ahmed, I. Hassan, M.F. El-Kady, A. Radhi, C.K. Jeong, P.R. Selvaganapathy, J. Zu, S. Ren, Q. Wang, R.B. Kaner, Integrated triboelectric nanogenerators in the era of the internet of things, Adv. Sci. 6 (2019) 1802230, https://doi.org/10.1002/advs.201802230.
[6] Q. Shi, T. He, C. Lee, More than energy harvesting − combining triboelectric nanogenerator and flexible electronics technology for enabling novel micro-/nano-systems, Nano Energ. 57 (2019) 851−871, https://doi.org/10.1016/j.nanoen.2019.01.002.
[7] Q. Shi, Z. Sun, Z. Zhang, C. Lee, Triboelectric nanogenerators and hybridized systems for enabling next-generation IoT applications, Res. 2021 (2021) 1−30, https://doi.org/10.34133/2021/6849171.
[8] M. Zhou, M.S.H. Al-Furjan, J. Zou, W. Liu, A review on heat and mechanical energy harvesting from human − principles, prototypes and perspectives, Renew. Sustain. Energ. Rev. 82 (2018) 3582−3609, https://doi.org/10.1016/j.rser.2017.10.102.
[9] H.-X. Zou, Mechanical modulations for enhancing energy harvesting_ Principles, methods and applications, Appl. Energy (2019) 18.
[10] J. Wang, L. Geng, L. Ding, H. Zhu, D. Yurchenko, The state-of-the-art review on energy harvesting from flow-induced vibrations, Appl. Energ. 267 (2020) 114902, https://doi.org/10.1016/j.apenergy.2020.114902.
[11] S. Bai, C. Liu, Overview of energy harvesting and emission reduction technologies in hybrid electric vehicles, Renew. Sustain. Energ. Rev. 147 (2021) 111188, https://doi.org/10.1016/j.rser.2021.111188.
[12] J. Pei, F. Guo, J. Zhang, B. Zhou, Y. Bi, R. Li, Review and analysis of energy harvesting technologies in roadway transportation, J. Clean. Prod. 288 (2021) 125338, https://doi.org/10.1016/j.jclepro.2020.125338.
[13] B. Maamer, A review on design improvements and techniques for mechanical energy harvesting using piezoelectric and electromagnetic schemes, Energ. Convers. Manag. (2019) 23.
[14] H. Ryu, H.-J. Yoon, S.-W. Kim, Hybrid energy harvesters: toward sustainable energy harvesting, Adv. Mater. 31 (2019) 1802898, https://doi.org/10.1002/adma.201802898.
[15] Y. Zhang, P.T.T. Phuong, E. Roake, H. Khanbareh, Y. Wang, S. Dunn, C. Bowen, Thermal energy harvesting using pyroelectric-electrochemical coupling in ferroelectric materials, Joule 4 (2020) 301−309, https://doi.org/10.1016/j.joule.2019.12.019.
[16] H. Liu, Hybrid energy harvesting technology: from materials, structural design, system integration to applications, Renew. Sustain. Energ. Rev. (2021) 25.
[17] N. Sezer, M. Koç, A comprehensive review on the state-of-the-art of piezoelectric energy harvesting, Nano Energ. 80 (2021) 105567, https://doi.org/10.1016/j.nanoen.2020.105567.
[18] C. Rodrigues, D. Nunes, D. Clemente, N. Mathias, J.M. Correia, P. Rosa-Santos, F. Taveira-Pinto, T. Morais, A. Pereira, J. Ventura, Emerging triboelectric nanogenerators for ocean wave energy harvesting: state of the art and future

perspectives, Energ. Environ. Sci. 13 (2020) 2657–2683, https://doi.org/10.1039/D0EE01258K.
[19] X. Chen, Z. Ren, M. Han, J. Wan, H. Zhang, Hybrid energy cells based on triboelectric nanogenerator: from principle to system, Nano Energ. 75 (2020) 104980, https://doi.org/10.1016/j.nanoen.2020.104980.
[20] Y. Song, N. Wang, C. Hu, Z.L. Wang, Y. Yang, Soft triboelectric nanogenerators for mechanical energy scavenging and self-powered sensors, Nano Energ. 84 (2021) 105919, https://doi.org/10.1016/j.nanoen.2021.105919.
[21] H. Yang, F.R. Fan, Y. Xi, W. Wu, Design and engineering of high-performance triboelectric nanogenerator for ubiquitous unattended devices, EcoMat 3 (2021), e12093, https://doi.org/10.1002/eom2.12093.
[22] H. Askari, Z. Saadatnia, A. Khajepour, M.B. Khamesee, J. Zu, A triboelectric self-powered sensor for tire condition monitoring: concept, design, fabrication, and experiments, Adv. Eng. Mater. 19 (2017) 1700318, https://doi.org/10.1002/adem.201700318.
[23] J. Wen, B. Chen, W. Tang, T. Jiang, L. Zhu, L. Xu, J. Chen, J. Shao, K. Han, W. Ma, Z.L. Wang, Harsh-environmental-resistant triboelectric nanogenerator and its applications in autodrive safety warning, Adv. Energ. Mater. 8 (2018) 1801898, https://doi.org/10.1002/aenm.201801898.
[24] J. Qian, D.-S. Kim, D.-W. Lee, On-vehicle triboelectric nanogenerator enabled self-powered sensor for tire pressure monitoring, Nano Energ. 49 (2018) 126–136, https://doi.org/10.1016/j.nanoen.2018.04.022.
[25] T. Guo, J. Zhao, W. Liu, G. Liu, Y. Pang, T. Bu, F. Xi, C. Zhang, X. Li, Self-powered Hall vehicle sensors based on triboelectric nanogenerators, Adv. Mater. Technol. 3 (2018) 1800140, https://doi.org/10.1002/admt.201800140.
[26] J. He, S. Cao, H. Zhang, Cylinder-based hybrid rotary nanogenerator for harvesting rotational energy from axles and self-powered tire pressure monitoring, Energ. Sci. Eng. 8 (2020) 291–299, https://doi.org/10.1002/ese3.560.
[27] Y. Du, Q. Tang, W. He, W. Liu, Z. Wang, H. Wu, G. Li, H. Guo, Z. Li, Y. Peng, C. Hu, Harvesting ambient mechanical energy by multiple mode triboelectric nanogenerator with charge excitation for self-powered freight train monitoring, Nano Energ. 90 (2021) 106543, https://doi.org/10.1016/j.nanoen.2021.106543.
[28] C. Bao Han, W. Du, C. Zhang, W. Tang, L. Zhang, Z. Lin Wang, Harvesting energy from automobile brake in contact and non-contact mode by conjunction of triboelectrification and electrostatic-induction processes, Nano Energ. 6 (2014) 59–65, https://doi.org/10.1016/j.nanoen.2014.03.009.
[29] H. Zhou, G. Liu, Y. Gao, Z. Wang, Y. Qin, Y. Wang, Y. Lin, Y. Xie, Y. Chen, C. Zhang, Dual mode rotary triboelectric nanogenerator for collecting kinetic energy from bicycle brake, Adv. Energ. Sustain. Res. 2 (2021) 2000113, https://doi.org/10.1002/aesr.202000113.
[30] S. Chatterjee, S. Saha, S.R. Barman, I. Khan, Y.-P. Pao, S. Lee, D. Choi, Z.-H. Lin, Enhanced sensing performance of triboelectric nanosensors by solid-liquid contact electrification, Nano Energ. 77 (2020) 105093, https://doi.org/10.1016/j.nanoen.2020.105093.
[31] J. Nie, Z. Ren, L. Xu, S. Lin, F. Zhan, X. Chen, Z.L. Wang, Probing contact-electrification-induced electron and ion transfers at a liquid–solid interface, Adv. Mater. 32 (2020) 1905696, https://doi.org/10.1002/adma.201905696.
[32] C.P. Vo, M. Shahriar, C.D. Le, K.K. Ahn, Mechanically active transducing element based on solid–liquid triboelectric nanogenerator for self-powered sensing, Int. J. Precis. Eng. Manuf.-Green Technol. 6 (2019) 741–749, https://doi.org/10.1007/s40684-019-00143-z.
[33] C. Zhang, L. Liu, L. Zhou, X. Yin, X. Wei, Y. Hu, Y. Liu, S. Chen, J. Wang, Z.L. Wang, Self-powered sensor for quantifying ocean surface water waves based on triboelectric nanogenerator, ACS Nano 14 (2020) 7092–7100, https://doi.org/10.1021/acsnano.0c01827.
[34] P. Wang, S. Zhang, L. Zhang, L. Wang, H. Xue, Z.L. Wang, Non-contact and liquid–liquid interfacing triboelectric nanogenerator for self-powered water/liquid level sensing, Nano Energ. 72 (2020) 104703, https://doi.org/10.1016/j.nanoen.2020.104703.
[35] D.L. Vu, C.D. Le, C.P. Vo, K.K. Ahn, Surface polarity tuning through epitaxial growth on polyvinylidene fluoride membranes for enhanced performance of liquid-solid triboelectric nanogenerator, Compos. B Eng. 223 (2021) 109135, https://doi.org/10.1016/j.compositesb.2021.109135.
[36] Z.L. Wang, A.C. Wang, On the origin of contact-electrification, Mater. Today 30 (2019) 34–51, https://doi.org/10.1016/j.mattod.2019.05.016.
[37] F. Zhan, A.C. Wang, L. Xu, S. Lin, J. Shao, X. Chen, Z.L. Wang, Electron transfer as a liquid droplet contacting a polymer surface, ACS Nano 14 (2020) 17565–17573, https://doi.org/10.1021/acsnano.0c08332.